Dynamically Feasible Task Space Planning for Underactuated Aerial Manipulators

Jake Welde, James Paulos, and Vijay Kumar

***Abstract*—In this work, we address the problem of planning dynamically feasible trajectories for underactuated aerial manipulators to achieve a desired trajectory for the end effector. We consider a quadrotor equipped with an arbitrary *n*-joint articulated arm. We show that the combined underactuated system is differentially flat, however the flat outputs do not correspond directly to the motion of the end effector. We therefore develop a method which determines the family of flat output trajectories which will exactly produce any desired task trajectory, even in the case of dynamic maneuvers. We also give criteria on the manipulator geometry which will ensure certain important stability properties, informing hardware design. The entire approach is demonstrated in simulation for systems of varying geometry and number of joints. The simultaneous resolution of the kinematic and dynamic constraints allows these tasks to be performed dynamically without sacrificing accuracy.**

***Index Terms*—Aerial systems: mechanics and control, underactuated robots, aerial manipulation, differential flatness, motion and path planning**

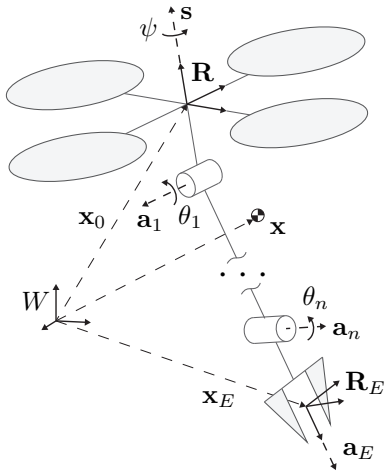

Fig. 1. Schematic of an aerial manipulator consisting of an underactuated aerial vehicle equipped with an n-joint articulated arm and end effector.

I. Introduction

AERIAL manipulation seeks to combine the dexterity, precision, and robustness of manipulator arms with the unbounded workspace and terrain independence of aerial vehicles. Over the last decade, there have been many exciting advances in both theory and experimental practice [1]. Teams of robots with body-fixed grippers have performed cooperative assembly tasks [2], and a quadrotor with a planar 2-DOF arm has been shown to transport small objects [3]. Many early examples of aerial manipulators leveraged underactuated vehicles such as quadrotors and had arms of only a few joints, but did not fully account for the dynamic coupling of the arm and the vehicle, limiting performance and precision. Recently, there has been a greater prevalence of systems employing:

- fully-actuated vehicle platforms, enabling independent translation and rotation of the vehicle [4][5][6]
- highly redundant manipulator arms, able to correct error as the slow, imprecise vehicle tracks a dynamically infeasible reference trajectory [7][8][9] in the spirit of a "macro-micro" manipulator [10]

However, these capabilities come at a price. Due to the physical limits of aerial vehicles, thrust is precious; to spend it supporting the weight of additional components makes it unavailable for dynamic maneuvers and reduces the endurance of the platform. The result is sluggish systems that strain to carry heavy actuators they may not need to complete the task.

In view of these characteristics, it is clear that lightweight underactuated vehicles with minimally jointed arms will outperform their redundant counterparts in terms of cost, endurance, and agility; the question is whether they can remain competitive in terms of dexterity and precision. We argue that the apparent shortcomings of underactuated aerial manipulators, in particular the tradeoff between precision and dynamic capabilities, can be largely resolved by planning trajectories which kinematically achieve the desired end effector motion while also satisfying the system's underactuated dynamics. This is especially vital when engaging in aggressive maneuvers or high-precision tasks, where dynamic feasibility is crucial to ensure accurate tracking. For example, in [11], an aerial manipulator spray painting line art could only perform the task with acceptable quality under quasi-static conditions.

Methods to plan dynamically feasible manipulation trajectories for simplified special cases have been demonstrated. A quadrotor with a body-fixed gripper was shown to grasp moving objects in simulation using manually designed dynamically feasible trajectories, but only for constant velocity targets [12]. A planar aerial manipulator with one joint moving

Manuscript received: October, 15, 2020; Accepted December, 13, 2020.

This paper was recommended for publication by Editor Pauline Pounds upon evaluation of the Associate Editor and Reviewers' comments. This work was supported by ARL Grant DCIST CRA W911NF-17-2-0181, NSF Grant CNS-1521617, ARO Grant W911NF-13-1-0350, ONR Grants N00014-20-1-2822 and ONR grant N00014-20-S-B001, Qualcomm Research, and C-BRIC, a Semiconductor Research Corporation Joint University Microelectronics Program program cosponsored by DARPA. The first author gratefully acknowledges support from the NSF Graduate Research Fellowship Program.

The authors are with the General Robotics Automation Sensing and Perception (GRASP) Laboratory at the University of Pennsylvania, Philadelphia, PA 19104 USA. {jwelde,jpaulos,kumar}@seas.upenn.edu

Digital Object Identifier (DOI): see top of this page.

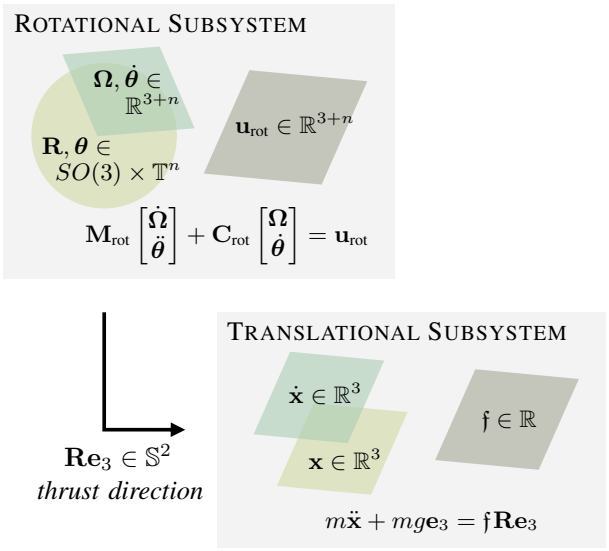

Fig. 2. The use of the system center of mass instead of the vehicle position in the configuration variables puts the equations of motion into an explicitly cascaded form, familiar from the dynamics of a quadrotor.

at high speeds was shown to grasp stationary objects [13], and a theoretical extension to planar systems with more joints has also been developed [14]. However, in addition to the planar restriction, both of these works required that the system have specific geometry that can be difficult to realize in hardware, namely that the arm be attached at the center of mass. Likewise, our prior work demonstrated dynamically feasible planning of the end effector pose trajectory in $SE(3)$ for a quadrotor with a 2-joint arm, but again only for manipulators with special geometry for which the system center of mass is static as viewed in the end effector reference frame [15].

In this work, we show that all aerial manipulators consisting of an underactuated vehicle and an articulated arm are differentially flat systems, such that we may minimally describe the space of permissible trajectories in terms of sufficiently smooth trajectories for the flat outputs. We then formulate and solve the dynamically feasible inverse kinematics problem, determining which flat output trajectories will exactly produce a desired trajectory for the end effector, despite the system's underactuation and kinematic redundancy. Using these results, we present two classes of aerial manipulators possessing key stability properties. Finally, in simulation we show the applicability of the method to a broad domain of problems requiring precision and dynamic performance.

II. System Definiton and Modeling

The class of systems in question is shown in Fig. 1, meant to represent a quadrotor equipped with a manipulator arm of arbitrary number of joints and geometry, including systems with $n = 0$ joints or $n = 1$ joint. We model the vehicle and each link of the arm as a rigid body, specifying the configuration and velocities of the system as

$$\mathbf{q} = \begin{Bmatrix} \mathbf{x} \\ \mathbf{R} \\ \boldsymbol{\theta} \end{Bmatrix} \in \mathbb{R}^3 \times SO(3) \times \mathbb{T}^n, \quad \mathbf{v} = \begin{bmatrix} \dot{\mathbf{x}} \\ \boldsymbol{\Omega} \\ \dot{\boldsymbol{\theta}} \end{bmatrix} \in \mathbb{R}^{6+n} \quad (1)$$

The chosen configuration variables are the global position $\mathbf{x} \in \mathbb{R}^3$ of the center of mass of the entire system (including the arm), the rotation $\mathbf{R} \in SO(3)$ from the vehicle frame to the world frame, and the tuple of joint angles $\boldsymbol{\theta} = \{\theta_1 \ \ldots \ \theta_n\} \in \mathbb{T}^n$ where $\theta_i \in \mathbb{S}^1$. For the velocities, $\dot{\mathbf{x}} \in \mathbb{R}^3$ is the center of mass velocity, $\boldsymbol{\Omega} \in \mathbb{R}^3$ is the body-frame angular velocity of the vehicle, and $\dot{\boldsymbol{\theta}} \in \mathbb{R}^n$ is the vector of joint velocities. The system has inputs $\mathbf{u} = \begin{bmatrix} \mathfrak{f} & \mathfrak{m}^{\mathrm{T}} & \mathfrak{t}^{\mathrm{T}} \end{bmatrix}^{\mathrm{T}} \in \mathbb{R}^{4+n}$, where $\mathfrak{f} \in \mathbb{R}$ is the magnitude of net rotor thrust, fixed in the $\mathbf{e}_3$ direction in the vehicle frame, $\mathfrak{m} \in \mathbb{R}^3$ is the net moment vector on the vehicle due to the rotors, and $\mathfrak{t} \in \mathbb{R}^n$ is the vector of applied joint torques. Appealing to the Lie group structure of the configuration manifold, we write the kinematics of the system as $\dot{\mathbf{q}} = \mathbf{q}\hat{\mathbf{v}}$, or in expanded explicit form as

$$\frac{d}{dt}\mathbf{x} = \dot{\mathbf{x}}, \quad \frac{d}{dt}\mathbf{R} = \mathbf{R}\hat{\boldsymbol{\Omega}}, \quad \frac{d}{dt}\boldsymbol{\theta} = \dot{\boldsymbol{\theta}} \quad (2)$$

where the notation $\hat{\cdot}$ is the overloaded *hat map* from Euclidean coordinates to the appropriate Lie algebra.

Consider the position $\mathbf{x}_i$ and orientation $\mathbf{R}_i$ of each rigid body in the system relative to the world frame W, where $i \in \{0, \ldots, n\}$ and $\mathbf{R}_0$ is simply $\mathbf{R}$. We remark that each body's global position and orientation may be expressed as

$$\mathbf{x}_i(\mathbf{q}) = \mathbf{x} + \mathbf{R}\,\mathbf{p}_i(\boldsymbol{\theta}), \quad \mathbf{R}_i(\mathbf{q}) = \mathbf{R}\,\mathbf{Q}_i(\boldsymbol{\theta}) \quad (3)$$

where $\mathbf{x}$ is the system center of mass position, $\mathbf{p}_i(\boldsymbol{\theta})$ is the displacement vector from the center of mass to body i expressed in the vehicle frame, and $\mathbf{Q}_i(\boldsymbol{\theta})$ gives the rotation from body i to the vehicle frame. Forward kinematics in this form may be derived by first following standard recursive methods using the vehicle position $\mathbf{x}_0$, then expressing the center of mass as a weighted sum,

$$m\mathbf{x} = m_0\mathbf{x}_0 + m_1\mathbf{x}_1 + \ldots + m_n\mathbf{x}_n \quad (4)$$

from which we may isolate $\mathbf{x}_0$ in terms of our chosen chosen configuration variables, substituting that result back into our expressions for $\mathbf{x}_i$ and $\mathbf{R}_i$ to reveal the form of (3).

Using the generalized Lagrangian method presented in [16], we derive globally valid, singularity-free equations of motion in the standard form of the manipulator equations,

$$\mathbf{M}(\mathbf{q})\,\dot{\mathbf{v}} + \mathbf{C}(\mathbf{q}, \mathbf{v})\,\mathbf{v} + \mathbf{g}(\mathbf{q}) = \mathbf{B}(\mathbf{q})\,\mathbf{u} \quad (5)$$

The choice of the system center of mass in the configuration, as opposed to the more obvious choice of the vehicle position, is deliberate. It has been shown that the dynamics of floating-base robots like aerial manipulators can be expressed in a decoupled form by transforming equations of motion derived in some naive representation into a sparse form where the center of mass position and velocity appear explicitly [7]. Informed by these results, we have chosen a state representation which effectively resolves this transformation at the kinematic level. The sparsity resulting from this choice will provide insight into the system structure and simplify implementation. In particular, the equations of motion (5) can be expanded as

$$\begin{bmatrix} m\mathbf{I}_3 & \mathbf{0} \\ \mathbf{0} & \mathbf{M}_{\text{rot}} \end{bmatrix} \dot{\mathbf{v}} + \begin{bmatrix} \mathbf{0} & \mathbf{0} \\ \mathbf{0} & \mathbf{C}_{\text{rot}} \end{bmatrix} \mathbf{v} + \begin{bmatrix} mg\mathbf{e}_3 \\ \mathbf{0} \end{bmatrix} = \begin{bmatrix} \mathbf{R}\mathbf{e}_3 & \mathbf{0} \\ \mathbf{B}_{\text{rot}} & \mathbf{I}_{3+n} \end{bmatrix} \mathbf{u} \quad (6)$$

where the submatrices have the sparse state dependencies

$$\mathbf{M}_{\text{rot}} = \mathbf{M}_{\text{rot}}(\boldsymbol{\theta}),\ \mathbf{B}_{\text{rot}} = \mathbf{B}_{\text{rot}}(\boldsymbol{\theta}),\ \mathbf{C}_{\text{rot}} = \mathbf{C}_{\text{rot}}(\boldsymbol{\theta}, \dot{\boldsymbol{\theta}}, \boldsymbol{\Omega}) \quad (7)$$

The effect of the thrust input on the rotational subsystem can easily be eliminated by a change of input variables. Therefore as seen in Fig. 2, the dynamics take the form of two cascaded subsystems; a fully actuated rotational subsystem evolves independently, feeding the direction of the thrust vector into the underactuated translational subsystem.

III. Differential Flatness

Widely utilized in the aerial robotics literature, *differential flatness* is a system property that allows us to describe the dynamically feasible trajectories of an underactuated system in a representation not subject to differential constraints [17]. Briefly, we say that a system is differentially flat if there exists some (non-unique) *flat output* $\mathbf{y} \in \mathcal{Y}$ such that the state and inputs can be expressed as a function of the flat output and a finite number of its derivatives, as

$$\{\mathbf{q}, \mathbf{v}, \mathbf{u}\} = \gamma(\mathbf{y}, \dot{\mathbf{y}}, \ldots, \mathbf{y}^{(r)}) \quad (8)$$

where the flat output must be given by a function

$$\mathbf{y} = \varphi(\mathbf{q}, \mathbf{v}, \mathbf{u}, \dot{\mathbf{u}}, \ldots, \mathbf{u}^{(s)}) \quad (9)$$

and the flat space and input space are of the same dimension.

The flat outputs must be differentially independent, meaning that there will be no dynamic feasibility requirements on trajectories in the flat space, other than smoothness of order r. Therefore, each sufficiently smooth trajectory in the flat space can be mapped to a dynamically feasible trajectory in the state-input space, enabling efficient trajectory planning and revealing the fundamental structure of the family of dynamically feasible trajectories for the system.

A. Configuration Manifold as a Fiber Bundle

As a preliminary, we analyze the topology of the configuration manifold. To begin, we recall the Hopf fibration, leveraged in [18] for the control of a standard quadrotor. Briefly, the Hopf fibration is the nontrivial fiber bundle

$$\mathbb{S}^1 \hookrightarrow \mathbb{S}^3 \xrightarrow{h} \mathbb{S}^2 \quad (10)$$

where h is a smooth surjective map projecting $\mathbb{S}^3$ onto $\mathbb{S}^2$. The notion is that the *total space* $\mathbb{S}^3$ is locally indistinguishable from the product of the *base space* $\mathbb{S}^2$ and the *fiber space* $\mathbb{S}^1$ (even though this is not the case globally), and $h^{-1}(\mathbf{s})$ (the fiber of total space "above" $\mathbf{s} \in \mathbb{S}^2$) is homeomorphic to $\mathbb{S}^1$.

A double cover $\mathbb{S}^3 \to SO(3)$ will reveal a related bundle

$$\mathbb{S}^1 \hookrightarrow SO(3) \xrightarrow{p} \mathbb{S}^2 \quad (11)$$

with $p(\mathbf{R}) = \mathbf{R}\mathbf{e}_3$. We may also construct a *local section* (in other words, a local right inverse of the bundle projection p) on some open set $\mathcal{O} \subset \mathbb{S}^2$ in the form $\sigma_p : \mathcal{O} \to SO(3)$ which assigns each element of $\mathcal{O}$ with an element in the fiber above it, such that $p \circ \sigma_p(\mathbf{s}) = \mathbf{s}$. Let us establish a smooth family of such sections parametrized by $\psi \in \mathbb{S}^1$, on the open set $\mathcal{O} \coloneqq \mathbb{S}^2 \setminus \{-\mathbf{e}_3\}$, constructed using the functions

$$\mathbf{H}_1 : \mathbb{S}^1 \to SO(3), \quad \mathbf{H}_2 : \mathbb{S}^2 \to SO(3) \quad (12)$$

derived from [18] as

$$\mathbf{H}_1(\psi) = \begin{bmatrix} \cos\psi & -\sin\psi & 0 \\ \sin\psi & \cos\psi & 0 \\ 0 & 0 & 1 \end{bmatrix} \quad (13)$$

$$\mathbf{H}_2(\mathbf{s}) = \begin{bmatrix} 1 - \frac{\mathrm{s}_1^2}{1+\mathrm{s}_3} & -\frac{\mathrm{s}_1\mathrm{s}_2}{1+\mathrm{s}_3} & \mathrm{s}_1 \\ -\frac{\mathrm{s}_1\mathrm{s}_2}{1+\mathrm{s}_3} & 1 - \frac{\mathrm{s}_2^2}{1+\mathrm{s}_3} & \mathrm{s}_2 \\ -\mathrm{s}_1 & -\mathrm{s}_2 & \mathrm{s}_3 \end{bmatrix} \quad (14)$$

Composing these rotations as

$$\mathbf{R} = \sigma_p(\mathbf{s}\,; \psi) \coloneqq \mathbf{H}_2(\mathbf{s})\,\mathbf{H}_1(\psi) \quad (15)$$

yields a family of sections describing any element $\mathbf{R} \in SO(3)$ with $p(\mathbf{R}) \neq -\mathbf{e}_3$ in terms of two specifications:

- a direction $\mathbf{s} \in \mathbb{S}^2$ to point the vector $\mathbf{e}_3 \in \mathbb{S}^2$
- a rotation around that vector by the angle $\psi \in \mathbb{S}^1$

The quadrotor's actuation geometry manifests this structure. If we point the thrust in some direction, we are left with a remaining degree of freedom rotating around that vector, together constructing the full orientation. Due to the product structure of the configuration manifold, it is straightforward to use the map $\pi(\mathbf{q}) = p \circ \text{proj}_2(\mathbf{q}) = p(\mathbf{R})$ to express the entire configuration manifold as the fiber bundle[1]

$$\mathbb{R}^3 \times \mathbb{T}^{n+1} \hookrightarrow \mathbb{R}^3 \times SO(3) \times \mathbb{T}^n \xrightarrow{\pi} \mathbb{S}^2 \quad (16)$$

abbreviated $\mathcal{Y} \hookrightarrow \mathcal{Q} \xrightarrow{\pi} \mathcal{S}$, where $\mathcal{Q}$ is the configuration manifold, $\mathcal{S}$ is the *shape space*, and it will be shown that $\mathcal{Y}$ is the flat space[2]. In particular, the flat outputs will be

$$\mathbf{y} = \begin{Bmatrix} \mathbf{x} \\ \boldsymbol{\theta}^+ \end{Bmatrix} \in \mathcal{Y} \quad (17)$$

where as before, $\mathbf{x} \in \mathbb{R}^3$ is the system's center of mass. $\boldsymbol{\theta}^+ = \begin{Bmatrix} \psi & \boldsymbol{\theta} \end{Bmatrix} \in \mathbb{T}^{n+1}$ is the tuple of physical joint angles augmented by the *virtual joint* around the thrust vector. We may also construct a corresponding family of sections as

$$\mathbf{q} = \sigma_\pi(\mathbf{s}\,; \mathbf{y}) \coloneqq \begin{Bmatrix} \mathbf{x} \\ \sigma_p(\mathbf{s}\,; \psi) \\ \boldsymbol{\theta} \end{Bmatrix} \quad (18)$$

and the local flat output map $\mathbf{y} = \varphi(\mathbf{q})$ can be given explicitly by extracting ψ in terms of $\mathbf{R}$ from (15), while the rest of the flat outputs are given by identity mappings. Then we may also define a *local trivialization* of the bundle using the homeomorphism $\Phi : \pi^{-1}(\mathcal{O}) \to \mathcal{O} \times \mathcal{Y}$ given by $\Phi(\mathbf{q}) = \{\pi(\mathbf{q}), \varphi(\mathbf{q})\}$, highlighting the local product structure of the configuration manifold.

B. Flatness Diffeomorphism

We must now give the state and inputs as functions of the flat outputs and their derivatives. In view of (18), if we can determine the shape $\mathbf{s}$ in terms of derivatives of the known flat outputs $\mathbf{y}$, we can immediately reconstruct the entire

[1]The function $\text{proj}_i : \mathcal{M}_1 \times \ldots \times \mathcal{M}_k \to \mathcal{M}_i$ is known as a *canonical projection*, mapping a product space onto its i^{th} factor.

[2]This system has the special property of *configuration flatness*, where the flat outputs depend only on the configuration and not the velocities or inputs.

configuration in terms of the flat output derivatives. Likewise, by differentiating (18) and invoking the kinematics we can also determine the velocities and accelerations, from which the inputs can be found with the equations of motion. Thus we seek to express the system's dynamic feasibility constraints in a form which we can solve to give the shape in terms of flat output derivatives.

A trajectory is dynamically feasible if and only if the necessary generalized forces lie in the *actuated subspace*, namely the column space of $\mathbf{B}$. This is evident in (5), since only when the left-hand side lies within the range of $\mathbf{B}$ can $\mathbf{u}$ be chosen to satisfy the equality. Equivalently, the required forces must be orthogonal to the *unactuated subspace*, such that the projection of the equations of motion onto this subspace takes the form

$$\left(\mathbf{B}_\perp\right)^{\mathrm{T}}\left(\mathbf{M}\dot{\mathbf{v}} + \mathbf{C}\mathbf{v} + \mathbf{g}\right) = \mathbf{0} \tag{19}$$

where $\mathbf{B}_\perp$ is a matrix whose columns span the left nullspace of $\mathbf{B}$ in all configurations. Because the rotational subsystem is fully actuated, it is easily verified that the choice

$$\mathbf{B}_\perp = \begin{bmatrix} \widehat{\mathbf{R}\mathbf{e}_3} \\ \mathbf{0}_{3+n\times 3} \end{bmatrix} \tag{20}$$

suffices, where we use the hat map to encode the cross product in the form of matrix multiplication. Note that $\operatorname{rank}\mathbf{B}_\perp = 2$, the degree of underactuation. Using the local trivialization and its derivatives to express the state and accelerations in terms of the shape and flat output derivatives, (19) will simplify to

$$\mathbf{s} \times (\ddot{\mathbf{x}} + g\mathbf{e}_3) = \mathbf{0} \tag{21}$$

which indicates that the thrust must point along the prescribed center of mass acceleration plus the effect of gravity, a familiar requirement from the case of the standard quadrotor [17]. The constraint (21) has two antipodal solutions for $\mathbf{s}$, and customarily we select the solution with strictly positive thrust[3],

$$\mathbf{s} = \frac{\ddot{\mathbf{x}} + g\mathbf{e}_3}{\|\ddot{\mathbf{x}} + g\mathbf{e}_3\|} \tag{22}$$

from which we reconstruct the entire configuration using (18). We then differentiate (21) twice, solving to give us the shape velocity and acceleration as

$$\dot{\mathbf{s}} = \frac{\left(\mathbf{I}_3 - \mathbf{s}\mathbf{s}^{\mathrm{T}}\right)\mathbf{x}^{(3)}}{\|\ddot{\mathbf{x}} + g\mathbf{e}_3\|} \tag{23}$$

$$\ddot{\mathbf{s}} = \frac{\left(\mathbf{I}_3 - \mathbf{s}\mathbf{s}^{\mathrm{T}}\right)\mathbf{x}^{(4)} - \left(2\dot{\mathbf{s}}\mathbf{s}^{\mathrm{T}} + \mathbf{s}\dot{\mathbf{s}}^{\mathrm{T}}\right)\mathbf{x}^{(3)}}{\|\ddot{\mathbf{x}} + g\mathbf{e}_3\|} \tag{24}$$

from which we may reconstruct $\mathbf{v}$ and $\dot{\mathbf{v}}$ via derivatives of the family of sections (18). Finally, we can find the inputs using the pseudoinverse[4] of $\mathbf{B}$ as

$$\mathbf{u} = \mathbf{B}^{\dagger}\left(\mathbf{M}\dot{\mathbf{v}} + \mathbf{C}\mathbf{v} + \mathbf{g}\right) \tag{25}$$

since we have already prescribed that the required generalized forces lie in the actuated subspace. Thus we have shown that this class of systems is always differentially flat, regardless of the particular geometry. Because we require $\ddot{\boldsymbol{\theta}}^+$ and $\mathbf{x}^{(4)}$ to determine the inputs, it must hold that $\boldsymbol{\theta}^+$ is $\mathcal{C}^2$ and $\mathbf{x}$ is $\mathcal{C}^4$ for there to exist a corresponding dynamically feasible trajectory for the physical system.

[3]Thus there exists two obverse diffeomorphisms centered around any chosen point in shape space—one for positive thrust and one for negative.

[4]For $\mathbf{B}$ with full column rank, $\mathbf{B}^{\dagger} = \left(\mathbf{B}^{\mathrm{T}}\mathbf{B}\right)^{-1}\mathbf{B}^{\mathrm{T}}$.

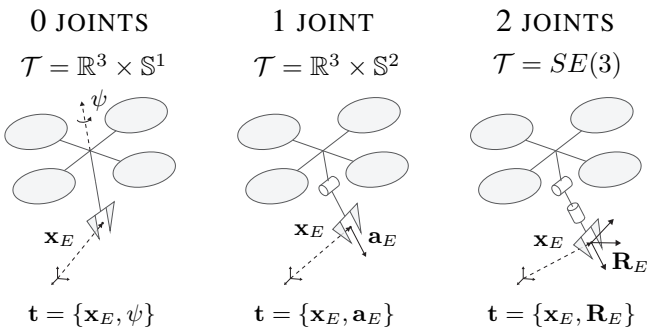

Fig. 3. The structure of the task space $\mathcal{T}$ depends on n, the number of joints in the arm. In the degenerate case where adjacent axes are parallel, a different definition should be adopted. Appropriate definitions for $n > 2$ will be determined by the application and thus are not considered here.

IV. Task Space Planning

A natural means of specifying a task for a manipulator is to describe the desired motion of its end effector via some suitable task outputs $\mathbf{t} \in \mathcal{T}$. Then, given a desired trajectory for $\mathbf{t}$, we must find the trajectories for the configuration $\mathbf{q}$ which all throughout satisfy the kinematic constraint

$$\tau(\mathbf{q}) = \mathbf{t} \tag{26}$$

where $\tau : \mathcal{Q} \to \mathcal{T}$ is the forward kinematic map. For fully-actuated manipulators, either minimal or redundant, this problem deals only with the manipulator geometry since any configuration trajectory is feasible. However, for underactuated systems, some trajectories for $\mathbf{q}$ which *kinematically* satisfy (26) may not be dynamically feasible, so cannot be executed.

We argue that the generalization of this problem to differentially flat systems is to determine trajectories for the flat outputs $\mathbf{y} \in \mathcal{Y}$ that produce the specified task motion for $\mathbf{t} \in \mathcal{T}$, since any such trajectory will be dynamically feasible. The appropriate task space will be of the same dimension as the flat outputs, and in Fig. 3 we show the natural choice for aerial manipulators of $n \in \{0, 1, 2\}$ joints, where for each case the task outputs consist of the position of the end effector $\mathbf{x}_E$ and some rotational information of varying dimension. Unfortunately, there will not in general exist a direct mapping between the flat outputs and the task outputs, because the task outputs will also depend on the shape.

A. Self-Motion Manifold

Due to the difference in dimension between the task space and configuration manifold, the kinematic structure of this problem resembles that of redundant, fully-actuated manipulators, wherein the subspace of the configuration manifold consistent with a prescribed task output is known as the *self-motion manifold*, on which the configuration may evolve

without affecting the task output [19]. For fully-actuated systems, the evolution on the self-motion manifold may be arbitrary, but for underactuated systems, even self-motion is subject to dynamic constraints.

To characterize the self-motion manifold, let us first divide the configuration manifold $\mathcal{Q}$ into open regular regions $\mathcal{Q}_i$, bounded by the critical value surfaces of the forward kinematic map, i.e. the physical manipulation singularities. In particular, the singularity for $n = 0$ is due to the singularity in the local trivialization at $\mathbf{s} = -\mathbf{e}_3$, while the other cases are of the same sort as the familiar *wrist singularity* occurring when axes align in a common plane. It can be shown that for each region, $\tau(\mathcal{Q}_i) = \mathcal{T}$, that is, each regular region has the entire task space as its range under the forward kinematic map. This can be seen by freezing the joints (since in the jointed case the critical value surfaces are given by critical values of the joint angles) and varying only the vehicle pose to cover all of $\mathcal{T}$.

We therefore remark that each regular region $\mathcal{Q}_i$ is a trivial fiber bundle over $\mathcal{T}$, with the forward kinematic map serving as the bundle projection [19]. Then, for the self-motion manifold of any $\mathbf{t} \in \mathcal{T}$, its component lying in $\mathcal{Q}_i$ is simply the fiber above $\mathbf{t}$. We also remark that over each $\mathcal{Q}_i$, the constraints

$$\tau(\mathbf{q}) = \mathbf{t}\,,\ \pi(\mathbf{q}) = \mathbf{s} \tag{27}$$

are independent, so for any prescribed task output, we may still choose the thrust direction. We will use this observation to construct a new family of sections for each $\mathcal{Q}_i$ in the form

$$\mathbf{q} = \sigma_\tau^i(\mathbf{t}\,;\mathbf{s}) \tag{28}$$

which, by varying the shape $\mathbf{s}$, describes the fiber above $\mathbf{t}$.

To derive these families of sections for each n, first consider the pose of the end effector in terms of the configuration a form directly analogous to (3), namely

$$\mathbf{x}_E = \mathbf{x} + \mathbf{R}\mathbf{p}_E(\boldsymbol{\theta}),\quad \mathbf{R}_E = \mathbf{R}\mathbf{Q}_E(\boldsymbol{\theta}) \tag{29}$$

and substitute $\mathbf{R} = \mathbf{H}_2(\mathbf{s})\,\mathbf{H}_1(\psi)$ from the family of sections (15). Clearly if we can determine ψ, we may reconstruct $\mathbf{R}$, and if we can determine $\boldsymbol{\theta}$, we may also find $\mathbf{x}$ as

$$\mathbf{x} = \mathbf{x}_E - \mathbf{R}\mathbf{p}_E(\boldsymbol{\theta}) \tag{30}$$

combining these results to construct the full task preimage.

Thus we consider the subproblem of determining the virtual and physical joint angles for each number of joints:

2: Beginning with the orientation constraint from (29), we move $\mathbf{H}_2(\mathbf{s})$ to the left side, yielding

$$\mathbf{H}_2(\mathbf{s})^{\mathrm{T}}\mathbf{R}_E = \mathbf{H}_1(\psi)\,\mathbf{Q}_E(\boldsymbol{\theta}) \tag{31}$$

This subproblem is equivalent to the inverse kinematics of a 3-joint wrist, which we may solve for ψ, θ_1, and θ_2 in terms of the prescribed $\mathbf{R}_E$ and $\mathbf{s}$.

1: Only the end effector axis $\mathbf{a}_E = \mathbf{R}_E\tilde{\mathbf{a}}_E$ is prescribed instead of the full orientation, so similarly:

$$\mathbf{H}_2(\mathbf{s})^{\mathrm{T}}\mathbf{a}_E = \mathbf{H}_1(\psi)\,\mathbf{Q}_E(\boldsymbol{\theta})\,\tilde{\mathbf{a}}_E \tag{32}$$

This subproblem is simply the inverse kinematics of a 2-joint wrist, which we likewise solve for ψ and θ_1.

0: ψ is given explicitly and there are no physical joints.

Using the other family of sections (15) to derive these solutions seems to introduce a singularity at $\mathbf{s} = -\mathbf{e}_3$. However, precisely the same singularity appears in the flatness diffeomorphism (and such a singularity must always exist by the Hairy Ball Theorem), therefore it is already present and will have no further deleterious effects on the final flat output trajectories.[5]

B. Simultaneous Resolution of Kinematic and Dynamic Constraints

To formulate the problem, we begin with the forward kinematic map (26) and substitute in the family of sections of the flatness bundle, expressing the kinematic constraint in terms of the flat outputs and the shape. By the definition of differential flatness, there are no feasibility constraints on the flat outputs other than smoothness, but the shape evolution is subject to the unactuated subspace constraint (21). Thus we are faced with the differential algebraic equation (DAE)

$$\tau \circ \sigma_\pi(\mathbf{s}\,;\mathbf{y}) = \mathbf{t} \tag{33a}$$

$$\mathbf{s} \times (\ddot{\mathbf{x}} + g\mathbf{e}_3) = \mathbf{0} \tag{33b}$$

where the first equation captures the algebraic (kinematic) constraints and the second equation captures the differential (dynamic) constraints.

Let us consider solutions over any particular $\mathcal{Q}_i$. Then applying the family of sections for the task bundle to the kinematic constraint (33a), followed by the flat output map, will yield a flat output trajectory in terms of the task outputs and the shape as

$$\mathbf{y} = \varphi \circ \sigma_\tau^i(\mathbf{t}\,;\mathbf{s}) \tag{34}$$

so all that remains is to find a shape profile which also satisfies the feasibility constraint (33b). However, the dynamic constraint on $\mathbf{s}$ depends itself on some flat output derivatives, namely $\ddot{\mathbf{x}}$. Let us therefore define the function

$$\mathbf{x} = \chi(\mathbf{t}\,;\mathbf{s}) \coloneqq \mathrm{proj}_1 \circ \varphi \circ \sigma_\tau^i(\mathbf{t}\,;\mathbf{s}) \tag{35}$$

expressing the subset of flat outputs whose derivatives appear in the unactuated subspace constraint in terms of the task outputs and the shape. Substituting this into (33b) gives us a second-order time-varying differential equation in $\mathbf{s}$,

$$\mathbf{s} \times \left(g\mathbf{e}_3 + \frac{d^2}{dt^2}\,\chi(\mathbf{t}\,;\mathbf{s})\right) = \mathbf{0} \tag{36}$$

subject to the simple geometric constraint

$$\mathbf{s} \in \mathbb{S}^2 \iff \mathbf{s}^{\mathrm{T}}\mathbf{s} = 1 \tag{37}$$

any solution of which describes a dynamically feasible configuration space trajectory via (34) in the minimal form of a flat output trajectory. For sufficiently well-behaved systems (to be made precise in Sec. V), the solution[6] to the initial value problem for initial conditions

$$\left\{\mathbf{s}_0, \dot{\mathbf{s}}_0\right\} \in T\mathbb{S}^2 \tag{38}$$

[5]A second diffeomorphism with a singularity elsewhere could easily be used to operate in this regime if necessary, as done in [18].

[6]Because the differential equation is highly nonlinear, we must find solutions numerically; to do so we expand the differential operator using the second-order chain rule and solve for the acceleration by also differentiating the geometric constraint. Integration in minimal coordinates using two antipodal stereographic projections dramatically improves solution accuracy.

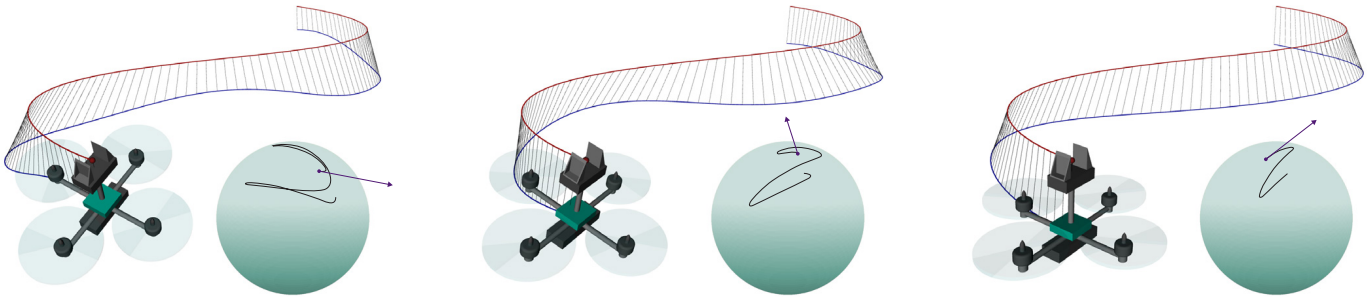

Fig. 4. The family of trajectories in the flat space which will exactly produce a desired task trajectory can be parametrized by the initial conditions of the shape dynamics *(in purple)*. Above are several different solutions *(in blue)* for the same task trajectory *(in red)* for a zero-joint system, along with the corresponding evolution in shape space *(in black)*. Solutions decrease in cost from left to right according to (40). Animations are shown in the video attachment.

is unique and exists on an arbitrary interval. The dimension of the initial conditions space is $2 \operatorname{rank} \mathbf{B}_\perp = 4$, where the factor of 2 arises due to the second derivative in the unactuated subspace constraint. In view of (34), these initial conditions parametrize the smooth finite-dimensional function space of solutions to the overall problem[7], as seen in Fig. 4. We also remark that the flatness of the system ensures controllability, such that the system can drive itself to the initial conditions required to execute a chosen solution.

C. Trajectory Optimization

Given the infinite space of solutions, we may consider a cost function to aid in the selection of a single solution, such as a running cost meant to minimize energy expenditure. The full state and inputs could be reconstructed to evaluate a more complex running cost, however this may be unnecessary. Letting $\mathbf{s}^\star(t)$ be the solution to the initial value problem for $\{\mathbf{s}_0, \dot{\mathbf{s}}_0\}$, we pose the minimization problem

$$\min_{\{\mathbf{s}_0, \dot{\mathbf{s}}_0\} \in T\mathbb{S}^2} \quad \int_0^T J\Big(\mathbf{s}^\star(t), \dot{\mathbf{s}}^\star(t), \ddot{\mathbf{s}}^\star(t)\Big)\, dt \tag{39}$$

with a task-appropriate running cost; for example,

$$J_2\big(\mathbf{s}, \dot{\mathbf{s}}, \ddot{\mathbf{s}}\big) = \Big|\Big|\ddot{\mathbf{s}}\Big|\Big|^2 \tag{40}$$

is very similar to the minimum snap cost used ubiquitously for quadrotors [17], since typically $\ddot{\mathbf{s}}$ is dominated by $\mathbf{x}^{(4)}$ as seen in (24). Because the dimension of the decision variables is very small, we can quickly find solutions to this shooting problem by numerical integration and gradient descent with a reasonable initial guess such as the hover condition. On a standard laptop, convergence occurs within seconds. Furthermore, the proposed formulation is an *anytime algorithm*, ideal for real-time planning: even if the optimization must be terminated early, the current best approximation specifies a trajectory that is both dynamically feasible and guaranteed to achieve the desired task motion, even if it may be suboptimal.

[7]The choice of some particular regular region $\mathcal{Q}_i$ also adds discrete multiplicity of the same sort we see in classical inverse kinematics.

V. Internal Dynamics

The result of the previous section is that the dynamic feasibility constraint has been expressed in a minimal and convenient form which does not restrict the motion in the task space; the task outputs may evolve arbitrarily, while the shape dynamics arising from (36) govern the evolution of the system on the self-motion manifold, as excited by the task motion. We refer to this as the *internal dynamics* due to resemblance to the method of input-output linearization [20].

This view highlights the risk that by exciting the internal dynamics, even some modest task motions might require very aggressive or even unbounded self-motions which will not be physically realizable, making even some mundane task motions impossible to perform. In [21], a zero-joint underactuated aerial manipulator was treated as a redundant mechanism by regulating only the position of the tool and not the yaw angle, leaving this last degree of freedom available to stabilize the internal dynamics, which otherwise may exhibit finite time escape. We adopt a different approach, which is to determine geometric criteria on the manipulator design which will prohibit the finite time escape of the internal dynamics, without sacrificing a dimension of manipulability. The stability of the internal dynamics (and naturally the avoidance of the physical manipulation singularities) is then the previously mentioned condition that the differential equation (36) be sufficiently well-behaved to guarantee existence and uniqueness of solutions to the initial value problem.

A. Internal Stability

Consider the problem of maintaining the task output at a constant value, a capability that any manipulator should have. We refer to the internal dynamics under such a condition as the *zero dynamics*, borrowing language again from input-output linearization. We note that expanding the second order derivative in (36) via chain rule will in general produce terms that are quadratic in $\dot{\mathbf{s}}$, such that the ODE expressed in state space form will not be globally Lipschitz. Thus finite time escape may occur even when keeping the task output constant, which is clearly unacceptable. However, recalling the function giving the center of mass in terms of the task outputs and shape defined in (35), it can be shown that if

$$\frac{\partial \chi}{\partial \mathbf{s}}(\mathbf{t}\,;\mathbf{s}) = -\lambda \mathbf{I}_3 \tag{41}$$

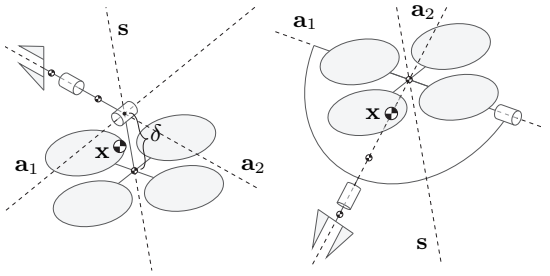

(a) *Stable Internal Dynamics* (b) *Task Flatness*

Fig. 5. Systems satisfying certain geometric criteria will enjoy favorable properties that ensure the internal state remains bounded.

for some constant $\lambda \neq 0$, then the quadratic terms will vanish from the zero dynamics, yielding the differential equation

$$\mathbf{s} \times \left(g\mathbf{e}_3 - \lambda \ddot{\mathbf{s}} \right) = \mathbf{0} \tag{42}$$

By invoking the geometric constraint (37) on $\mathbf{s}$, we can solve for the zero dynamics in the form

$$\ddot{\mathbf{s}} = -\frac{g}{\lambda} \hat{\mathbf{s}}^2 \mathbf{e}_3 - \left|\left| \dot{\mathbf{s}} \right|\right|^2 \mathbf{s} \tag{43}$$

which resembles the dynamics of an undamped spherical pendulum. We therefore consider the energy-inspired function

$$H(\mathbf{s}, \dot{\mathbf{s}}) = -\frac{g}{\lambda} \mathbf{e}_3^{\mathsf{T}} \mathbf{s} + \frac{1}{2} \dot{\mathbf{s}}^{\mathsf{T}} \dot{\mathbf{s}} \tag{44}$$

which can be shown to be the Hamiltonian of the system with $\dot{H} = 0$, so the zero dynamics do not exhibit finite time escape since H is radially unbounded.[8] The system has equilibria at $\left\{ \mathbf{s}, \dot{\mathbf{s}} \right\} = \left\{ \pm \mathbf{e}_3, \mathbf{0} \right\}$, and it is easily verified using the Hamiltonian that the zero dynamics are globally stable in the sense of Lyapunov around the equilibrium with $\mathbf{s} = \operatorname{sgn}(\lambda)\, \mathbf{e}_3$, while the other equilibrium is unstable, similar to the stability result given in [21] for aerial manipulators of $n = 0$ joints.

Underactuated aerial manipulators whose physical and virtual joint axes all intersect at a common point, in the spirit of a *spherical wrist*, will have the property (41), so long as both this intersection point and the center of mass of each arm link can be expressed directly in terms of the task outputs. Such a system is shown in Fig. 5a, and in general $\lambda = \frac{m_0}{m} \delta$, where δ is the signed distance along the thrust vector from the vehicle position to the intersection point. The systems shown in Figs. 3 and 4 also have this property. Choosing geometry with $\lambda > 0$ (where the intersection is above the vehicle body's center of mass) is preferred due to the singularities in the local trivialization and in the flatness diffeomorphism (occurring when the thrust vanishes). We want to remain local to the hover equilibrium, avoiding inversion of the vehicle, so that for typical trajectories, thrust remains positive.

[8]Using the Hamiltonian of the zero dynamics, we may also demonstrate that even the internal dynamics excited by an arbitrary task trajectory cannot escape in finite time. It can be shown that, for large shape velocities, the generalized power $\dot{H}$ injected into the internal subsystem is bounded by H as long as the task output derivatives are bounded. Then the comparison principle will show that finite time escape may not occur, and thus for any finite duration task output trajectory with any shape initial conditions, the internal state will remain bounded. We omit the full derivation here due to space constraints.

B. Task Flatness

Now, consider systems with the special property

$$\frac{\partial \chi}{\partial \mathbf{s}}(\mathbf{t}\,; \mathbf{s}) = \mathbf{0} \tag{45}$$

namely the case where the center of mass can be expressed exclusively in terms of the task outputs with no dependence on the shape. Then, the internal dynamics vanish as (36) collapses into an algebraic constraint, which we solve for $\mathbf{s}$ in terms of derivatives of $\mathbf{t}$ and then explicitly reconstruct the flat output trajectory. The existence of such a mapping means that unlike in the general case, the solution family will be finite and discrete. Therefore, the task outputs of such a system constitute another valid choice of local flat outputs for the system, with the valid region bounded by the manipulation singularities. It can be verified that $\mathcal{C}^4$ smoothness of $\mathbf{t}$ will be sufficient, as it was for the flat outputs. Because such manipulators are locally differentially flat with respect to the task outputs, we call this property *task flatness*.

For the task flatness condition (45) to hold for systems with $n \in \{0, 1, 2\}$ joints, the center of mass $\mathbf{x}$ must be fixed in the end effector frame. For $n = 1$ it must also hold that $\mathbf{x}$ lies along the end effector axis $\mathbf{a}_E$, while for $n = 0$, $\mathbf{x}$ must be at the end effector frame origin such that $\mathbf{x} = \mathbf{x}_E$. Then in each case, fixing the task outputs will fully determine the global position of the center of mass. To ensure that the system center of mass will be static in the end effector frame, all bodies inboard of any given joint must have their combined center of mass located along that joint's axis. One example of such an aerial manipulator is shown in Fig. 5b. We also remark that the geometric requirements imposed in previous work [13][14][15] to show differential flatness of special classes of aerial manipulators with respect to practically convenient flat outputs are essentially task flatness criteria when viewed through the lens of our formulation.

Task flatness is a useful property, and these requirements may be seen as design criteria for particularly nice aerial manipulators. Task flatness precludes the existence of poorly behaved internal dynamics, while also affording all the standard benefits of planning in the flat space; constraints in the state-input space can be mapped to constraints on flat output derivatives, efficiently encoding actuator saturation limits, obstacle avoidance, and physical manipulation singularities without integration. Task flatness also guarantees that periodic trajectories in the task space will always map to periodic trajectories in configuration space.

VI. Simulations

The entire approach was implemented in simulation for a variety of aerial manipulator platforms and tasks. The flatness diffeomorphism was verified by simulating the open-loop dynamics under inputs corresponding to aggressive flat output trajectories, showing precise agreement with the nominal trajectory. To demonstrate the usefulness of agile manipulation, we plan a dynamically feasible trajectory for a quadrotor with a body-fixed gripper to grasp a small object moving quickly along a curved path. We also simulate spray painting a pattern on the curved surface of an elevated structure using a system

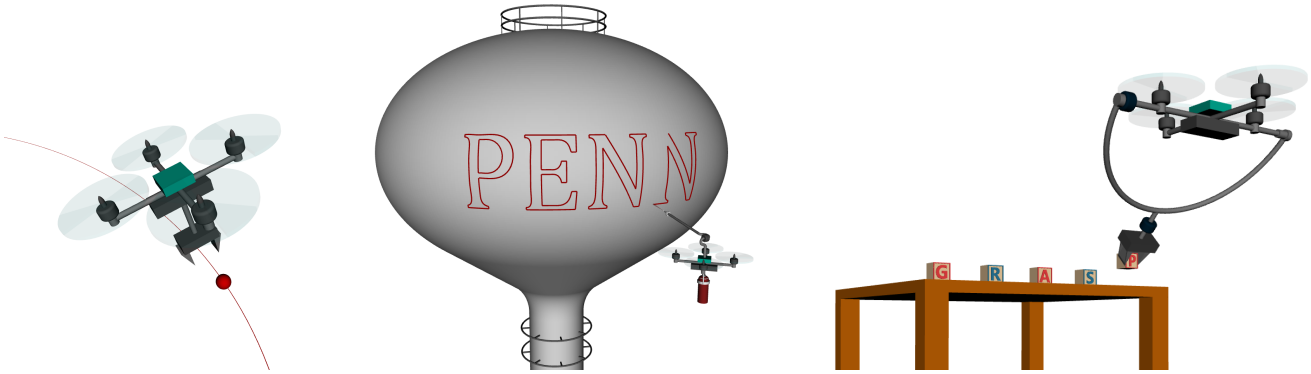

Fig. 6. We plan dynamically feasible trajectories to perform several aerial manipulation tasks: the dynamic grasping of a moving object, precision spray painting, and 6-DOF pick and place. More details are given in the video attachment, also available in higher quality at `www.jakewelde.com/ral2021`.

with one joint, motivating the importance of dynamic feasibility when error tolerance is small. Finally, we demonstrate the benefits of leveraging the vehicle agility to maximize manipulability by planning 6-DOF pick and place trajectories for a two-joint system. These simulations are shown in detail in the video attachment, as well as briefly in Fig. 6. In these simulations, we do not consider the exchange of forces between the system and objects in the environment, leaving them to be rejected by closed loop tracking control in implementation. This assumption is reasonable when performing pick and place tasks with small objects or when performing tasks that do not require physical contact.

VII. Conclusion

In summary, we have demonstrated that all underactuated aerial vehicles equipped with articulated manipulators are differentially flat systems regardless of their geometry. We have developed a new method for determining the family of dynamically feasible trajectories which will produce a desired end effector trajectory, allowing lightweight underactuated systems to perform dynamic maneuvers accurately. We have also determined criteria for a class of aerial manipulators whose internal dynamics are guaranteed to be well behaved, and another class for which the task outputs are themselves alternate flat outputs of the system, each providing design specifications for hardware platforms. Our future work will address integration with closed loop control and implementation on hardware, as well as the consideration of changing modes of environmental contact and exerting non-negligible external wrenches while retaining dynamic feasibility.

References

[1] X. Ding, P. Guo, K. Xu, and Y. Yu, "A review of aerial manipulation of small-scale rotorcraft unmanned robotic systems," *Chinese Journal of Aeronautics*, vol. 32, no. 1, pp. 200–214, jan 2019.

[2] F. Augugliaro, *et al.*, "The Flight Assembled Architecture installation: Cooperative construction with flying machines," *IEEE Control Systems Magazine*, vol. 34, no. 4, pp. 46–64, 2014.

[3] S. Kim, S. Choi, and H. J. Kim, "Aerial manipulation using a quadrotor with a two DOF robotic arm," *IEEE International Conference on Intelligent Robots and Systems*, pp. 4990–4995, 2013.

[4] M. Á. Trujillo, J. R. Martínez-De Dios, C. Martín, A. Viguria, and A. Ollero, "Novel aerial manipulator for accurate and robust industrial NDT contact inspection: A new tool for the oil and gas inspection industry," *Sensors*, vol. 19, no. 6, pp. 1–24, 2019.

[5] K. Bodie, *et al.*, "An Omnidirectional Aerial Manipulation Platform for Contact-Based Inspection," in *Robotics: Science and Systems*, Freiburg im Breisgau, 2019.

[6] M. Tognon, *et al.*, "A Truly-Redundant Aerial Manipulator System with Application to Push-and-Slide Inspection in Industrial Plants," *IEEE Robotics and Automation Letters*, vol. 4, no. 2, pp. 1846–1851, 2019.

[7] G. Garofalo, F. Beck, and C. Ott, "Task-space Tracking Control for Underactuated Aerial Manipulators," *2018 European Control Conference, ECC 2018*, pp. 628–634, 2018.

[8] G. Heredia, *et al.*, "Control of a multirotor outdoor aerial manipulator," *IEEE International Conference on Intelligent Robots and Systems*, pp. 3417–3422, 2014.

[9] G. Zhang, *et al.*, "Grasp a moving target from the air: System control of an aerial manipulator," *Proceedings - IEEE International Conference on Robotics and Automation*, pp. 1681–1687, 2018.

[10] A. Sharon, N. Hogan, and D. Hardt, "The Macro/Micro Manipulator: An Improved Architecture for Robot Control," *IEEE Transactions on Robotics and Automation*, vol. 10, no. 3, pp. 209–222, 1988.

[11] A. S. Vempati, *et al.*, "PaintCopter: An autonomous UAV for spray painting on three-dimensional surfaces," *IEEE Robotics and Automation Letters*, vol. 3, no. 4, pp. 2862–2869, 2018.

[12] R. Spica, A. Franchi, G. Oriolo, H. H. Bulthoff, and P. R. Giordano, "Aerial grasping of a moving target with a quadrotor UAV," *IEEE International Conference on Intelligent Robots and Systems*, pp. 4985–4992, 2012.

[13] J. Thomas, G. Loianno, J. Polin, K. Sreenath, and V. Kumar, "Toward autonomous avian-inspired grasping for micro aerial vehicles," *Bioinspiration and Biomimetics*, vol. 9, no. 2, 2014.

[14] B. Yüksel, G. Buondonno, and A. Franchi, "Differential flatness and control of protocentric aerial manipulators with any number of arms and mixed rigid-/elastic-joints," *IEEE International Conference on Intelligent Robots and Systems*, vol. 2016-Novem, pp. 561–566, 2016.

[15] J. Welde and V. Kumar, "Coordinate-Free Dynamics and Differential Flatness of a Class of 6DOF Aerial Manipulators," *International Conference on Robotics and Automation*, 2020.

[16] P. J. From, "An Explicit Formulation of Singularity-Free Dynamic Equations of Mechanical Systems in Lagrangian Form- Part Two: Multibody Systems," *Modeling, Identification and Control*, vol. 33, no. 2, pp. 61–68, 2012.

[17] D. Mellinger and V. Kumar, "Minimum Snap Trajectory Generation and Control for Quadrotors," *International Conference on Robotics and Automation*, pp. 2520–2525, 2011.

[18] M. Watterson and V. Kumar, "Control of Quadrotors Using the Hopf Fibration on SO(3)," in *Robotics Research*, 2020, pp. 199– 215.

[19] D. DeMers and K. Kreutz-Delgado, "Global Regularization of Inverse Kinematics for Redundant Manipulators," *Advances in Neural Information Processing Systems*, vol. 5, pp. 255—-262, 1993.

[20] H. K. Khalil, *Nonlinear Systems*. Upper Saddle River: Prentice Hall, 2002.

[21] H. N. Nguyen, C. Ha, and D. Lee, "Mechanics, control and internal dynamics of quadrotor tool operation," *Automatica*, vol. 61, 2015.